Science of the Total Environment 862 (2023) 160856

Contents lists available at ScienceDirect

Science of the Total Environment

journal homepage: www.elsevier.com/locate/scitotenv

The biophysical climate mitigation potential of riparian forest ecosystems in arid Northwest China

Su Yonghong [a,b,*], Luo Fandi [c,**], Zhu Gaofeng [d], Kun Zhang [e,f], Zhang Qi [a]

[a] Key Laboratory of Eco-hydrology of Inland River Basin (CAS), Northwest Institute of Eco-Environment and Resources, CAS, Lanzhou 730000, China
[b] College of Resources and Environment, University of Chinese Academy of Sciences, Beijing 100049, China
[c] School of Life Sciences, Lanzhou University, Lanzhou 730000, China
[d] College of Earth and Environmental Sciences, Lanzhou University, Lanzhou 730000, China
[e] Department of Mathematics, The University of Hong Kong, Hong Kong, China
[f] School of Biological Sciences, The University of Hong Kong, Hong Kong, China

HIGHLIGHTS

- Forest absorbed more radiation compared the desert background.
- The riparian forest was cooler in the summer and slightly warmer in winter.
- Biophysical factors contributing to surface temperature differences were evaluated.
- Surface temperature differences were mainly driven by surface albedo, incoming longwave radiation and evapotranspiration.
- A shallower, cooler and wetter boundary layer developed over forest in summer.

GRAPHICAL ABSTRACT

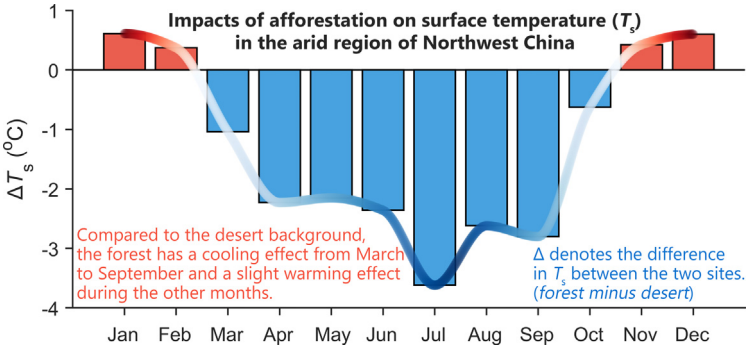

ARTICLE INFO

Editor: Daniel Alessi

Keywords:
Riparian forest, arid regions
Surface temperature
Biophysical processes
Planetary boundary layer

ABSTRACT

Forests influence climate through both the biochemical and biophysical processes, and the impacts of the latter on local climate may be much larger than the former. However, the biophysical effects of afforestation in arid regions have received little attention compared with afforestation in the tropic, temperate and boreal zones. In this study, we combined in situ eddy covariance flux measurements from a neighboring pairs of forested and background desert sites with the decomposed temperature metric (DTM) method to characterize the impacts of arid forests on surface temperature (T_s). A clear-sky, one-dimensional planetary boundary layer (PBL) model was used to estimate the impacts of afforestation on state of regional climate. We showed that despite absorbing more net radiation (35.4 W m^{-2}) the riparian forests tended to cool T_s (−1.28 °C) on annual basis, but with a significant seasonality. Specifically, afforestation may lead to a net cooling effect from March to September and a slightly warming effect in other months. The DTM method revealed that evapotranspiration played a dominant role in cooling surface temperature, while surface albedo (α) and incoming longwave radiation ($L\downarrow$) acted together to increase forest surface temperature. From June to September, a shallower, cooler and wetter boundary layer was developed over the forest due to high plant transpiration. In other months, the PBL was slightly deeper and warmer over the forest than that over the desert. Therefore, the riparian forests were important in moderating warming trends in arid regions.

* Correspondence to: S. Yonghong, Key Laboratory of Eco-hydrology of Inland River Basin (CAS), Northwest Institute of Eco-Environment and Resources, CAS, Lanzhou 730000, China.
** Corresponding author.
E-mail addresses: syh@lzb.ac.cn (S. Yonghong), luofd20@lzu.edu.cn (L. Fandi).

http://dx.doi.org/10.1016/j.scitotenv.2022.160856
Received 24 August 2022; Received in revised form 22 October 2022; Accepted 7 December 2022
Available online 12 December 2022

1. Introduction

Forests play a critical role in the Earth's climate system by sequestering C (biogeochemical effect) (Heimann and Reichstein, 2008; Alkama and Cescatti, 2016), and modulating the land-atmosphere exchange of energy and water vapor (biophysical effects) (Bonan, 2008; Burakowski et al., 2018). Compared with the biogeochemical effects, the biophysical effects are much more complicated and depend on regional climate conditions (Peng et al., 2014; Li et al., 2015; Wang et al., 2018). Additionally, the biophysical effects of forests on local climate can be much larger than the small global cooling effect resulting from forest C sequestration (Bala et al., 2007; Anderson et al., 2011). Therefore, an improved understanding of the impacts of biophysical processes on climate is necessary to guide policy decisions that support global climate mitigation, climate negotiations, local adaptation and biodiversity conservation (Anderson et al., 2011; Alkama and Cescatti, 2016; Lawrence et al., 2022).

To date, great efforts have been made in assessing the impacts of biophysical processes on climate. However, there still are some insufficiencies and uncertainties in estimated climate sensitivities to the ongoing forest changes (Alkama and Cescatti, 2016). First, the majority of previous studies on biosphere-atmosphere interactions mainly focused on forests in the tropical, temperate, and boreal regions (Lean and Warrilow, 1989; Bonan et al., 1992; Bonan, 2008; Betts, 2000; Lee et al., 2011; Peng et al., 2014; Wang et al., 2018). The biophysical impacts of forest in arid regions are currently ignored by the scientific community (Alkama and Cescatti, 2016). Due to their large size (~17.7 % of land surface occupied by arid/semi-arid forest) and high surface shortwave radiation conditions (Lal, 2004; Rotenberg and Yakir, 2010), obtaining direct observations of surface temperature changes associated with afforestation from these regions is principally important. Second, because of the high spatial heterogeneity of biophysical processes, the contribution of different biophysical factors (i.e., albedo, surface roughness and evapotranspiration) to climate signal (warming or cooling) varied with latitude, precipitation, water availability, species composition, and other characteristics (Rotenberg and Yakir, 2010; Lee et al., 2011; Peng et al., 2014; Zhang et al., 2014; Wang et al., 2018). For example, the drastic decrease in surface albedo causes boreal forests warm climate (Bonan et al., 1992; Betts, 2000), and high evapotranspiration rate makes tropic forests decrease surface temperature (Lean and Warrilow, 1989; Findell et al., 2006; Lawrence and Vandecar, 2015; Li et al., 2022). In other regions (especially for the arid areas), it is still not clear which of the biophysical factors contributes the most to changes in surface temperature (Rotenberg and Yakir, 2010; Lee et al., 2011; Peng et al., 2014; Zhang et al., 2014; Wang et al., 2018). Thus, there is a need to diagnose the effects of each individual biophysical factor on climate in these regions. Finally, despite surface temperature being important for all living organisms within (De Frenne et al., 2013), it fails to capture the effects of afforestation on local to regional climate (Luyssaert et al., 2014), and assessing the impacts of biophysical processes on the state of the low atmosphere is required.

Based on in situ observations made in a riparian forest and an adjacent desert site and a clear-sky, one-dimension planetary boundary layer (PBL) model, we investigated the biophysical effects of afforestation on climate in arid Northwest China. We aimed to: (1) investigate the impacts of afforestation on surface temperature in arid regions; (2) to quantify the contributions of individual biophysical factors to surface temperature changes associated with afforestation; and (3) estimate potential effects of vegetation cover changes on the states of the low atmosphere.

2. Materials and methods

2.1. Site Characteristics

The study site is located in the Ejina basin (40.17°-42.67° N, 99.5°-101.67° E; elevations ranging from 890 to 1127 m above sea level), Inner Mongolia Autonomous Region, China (Fig. 1). It is confined by the Badain Jaran

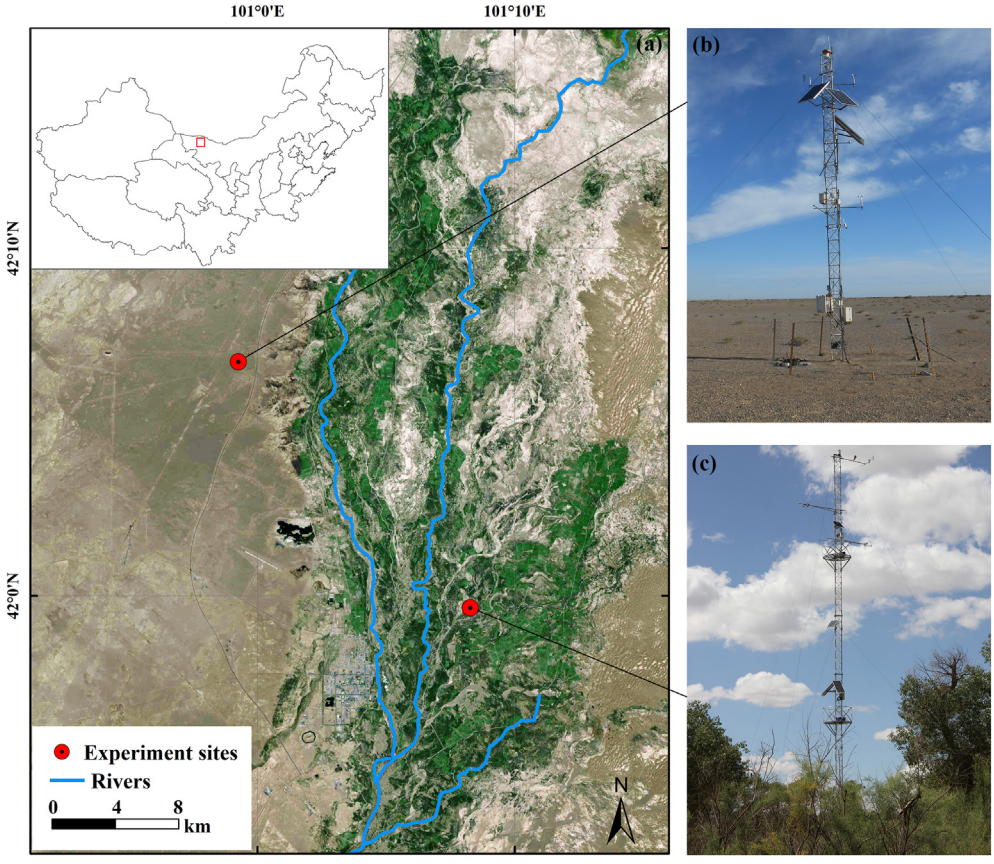

Fig. 1. (a) Locations; (b) and (c) pictures of the desert site and forest site, respectively.

Desert to the east and by mountains to both the west and north, which covers 3×10^4 km^2 with an oasis area 0.15×10^4 km^2 (Su et al., 2007). Being in the hinterland of Asian continent, the region is one of the most arid areas in the world and has an obvious characteristic of a continental climate. The mean annual precipitation is 42 mm, with the majority of rainfall (about 60–70 %) occurring between July to September (Su et al., 2022a, 2022b). The pan evaporation is as high as 2241 mm according to data collected for the period 1957–2016 from the Ejina Meteorological station (Si et al., 2015). The mean annual temperature is 8.9 °C, with a mean January temperature of −11.5 °C and a mean July temperature of 27.0 °C. Due to sparse precipitation, no perennial runoff originates from the area. The Heihe River, originating from the Qilian mountains of Qinghai provinces, is the only surface runoff in this area. It flows from south to north and finally reaches the terminal lakes. Native riparian forests widely distributed near the river banks and lake shore.

To evaluate the biophysical effects of afforestation on climate, we established two eddy covariance flux sites at the Sidaoqiao *P. euphratica* Forest National Natural Refuge (101.14° E, 42.00° N; 874 m elevation) and at the Gobi desert (100.99°E, 42.11°N, 1054 m elevation). This field observation was a part of the Heihe Watershed Allied Telemetry Experiment Research (HiWATER) project (Li et al., 2013). All sites, the instruments and the experimental procedures have been described in previous studies (Liu et al., 2016; Xu et al., 2017, 2020). We will only give a brief outline here.

The desert site is a nearly flat, open land surface that is covered with coarse-grain sand and small pebbles with withered sparse scrub grasses and herbs (Fig. 1b). Its communities are drought-tolerant species, such as severely degraded *Reaumuria soongorica*, *Salsola passerina*, and *Sympegma regelii*. The groundwater depth is >4 m, and plants mainly depend on atmospheric precipitation and condensation water for survival (Wang et al., 2002). The community in the forest site is composed of *Populus euphratica Oliv*. (*P. euphratica*) and *Tamarix ramosissima Ledeb*. (*T. ramosissima*) (Fig. 1c). The *P. euphratica* is the dominant plant species with a density of 320 stems ha^{-1}. The tree height and canopy coverage is 10.1 ± 1.7 m and 52 %, respectively. According to the soil texture classification standard of US Department of Agriculture (USDA), the soil texture profiles were silt loam with a clay interlayer (Wang et al., 2022). The mean groundwater depth was 1.9 m, and the growth and development of these species mainly depend on groundwater (Su et al., 2022a, 2022b).

2.2. Eddy covariance measurements and processing

We used the eddy covariance (EC) method to measure continuous fluxes of CO_2, latent heat and sensible heat at the two sites (Li et al., 2013; Xu et al., 2020). The turbulent fluxes were measured at the heights of 28 m and 4.7 m above the surface at the forest and desert sites, respectively. Fluxes were measured at a frequency of 10 Hz, using an open-path infrared gas analyzer (Li-7500, LiCor Inc., Lincoln, NE, USA) and a 3-D sonic anemometer (CSAT-3, Campbell Scientific Inc., Logan, UT, USA). The Edire software was used to process the raw EC data (http://www.geos.ed.ac.uk/abs/research/micromet/EdiRe/), which included spike detection, time lag correction, converting sonic temperature into actual temperature, coordinate rotation, the WPL (Webb-Pearman-Leuning) density fluctuation correction and frequency response correction (Xu et al., 2017). Energy balance closure serves as a metric to evaluate flux measurements when using the EC method over terrestrial ecosystems (Foken, 2008). About 10 % energy imbalance was found in our EC data (Xu et al., 2017), and the Bowen ratio correction method was used to reduce the imbalance (Foken, 2008). Continuous complementary measurements also included standard hydro-meteorological variables, such as rainfall, air temperature, relative humidity, downward and upward shortwave and longwave radiation, soil temperature and moisture, and soil heat fluxes. Detailed information about the instruments used in this study is listed in Table 1, and these in situ observations were all averaged to 30 min intervals.

The surface temperature (T_s; K) over the forest and desert sites was calculated from the upward longwave radiation flux ($L\uparrow$; W m^{-2}) and corrected for the surface reflection of downward longwave radiation flux ($L\downarrow$; W m^{-2}) (Wang et al., 2018):

$$T_s = \left(\frac{L\uparrow - (1-\varepsilon)L\downarrow}{\varepsilon\sigma}\right)^{\frac{1}{4}} \quad (1)$$

where ε is surface emissivity (assumed to be 0.98 here); and σ is the Stephan-Boltzmann constant (5.67×10^{-8} W m^{-2} K^{-4}). The surface albedo (α), a key component of the surface energy balance, is calculated as (Betts, 2001):

$$\alpha = \frac{K\downarrow}{K\uparrow} \quad (2)$$

where $K\downarrow$ is incoming shortwave radiation flux incident on the surface (W m^{-2}), $K\uparrow$ is the reflected shortwave radiation (W m^{-2}). The net surface shortwave radiation is then given by $S = (1\text{-}\alpha)\, K\downarrow$. To get some improvement in representivity, we generated daily mean values by averaging the 30-min in situ data. Daily average values of albedo (α) and surface temperature (T_s) were calculated from the daily average downward and upward shortwave and longwave radiation for each site. Then, monthly ensemble-averaged α and T_s were obtained from these daily values.

2.3. Decomposition of surface temperature changes

We apply the decomposed temperature metric (DTM) method to isolate the contributions to changes in surface temperature from individual biophysical factors of vegetation cover change (Juang et al., 2007; Luyssaert et al., 2014). The DTM method is based on surface energy balance:

$$R_n = S + L\downarrow - \varepsilon\sigma T_s^4 = H + \lambda E + G + I \quad (3)$$

where R_n is net radiation (W m^{-2}); S is net surface shortwave radiation (W m^{-2}); H is sensible heat flux (W m^{-2}); λE is latent heat flux (W m^{-2}); G is ground heat flux (W m^{-2}); and I is a residual imbalance

Table 1
Detailed station information for the EC and hydro-meteorological variable observations used in this study.

Variable	Forest site		Desert site	
	Sensors	Height & depth (m)	Sensors	Height & depth (m)
Sensible, latent heat and carbon dioxide flux (EC)	CSAT3 & Li7500A, Campbell & Li-Cor, USA	28	CSAT3 & Li7500A, Campbell & Li-Cor, USA	4.7
Wind speed/direction	Windsonic, Gill, UK	28	Windsonic, Gill, UK	5
Air temperature/humidity	HMP45D, Vaisala, Finland	28	HMP45AC, Vaisala, Finland	5
Four-component radiation (incoming/outgoing shortwave and longwave radiation, net radiation)	CNR4, Kipp & Zonen, Netherland	24	CNR1, Kipp & Zonen, Netherland	6
Soil heat flux	HFP01, Hukseflux, Netherland	0.06	HFT3, Campbell, USA	0.06
Soil temperature/moisture profile	AV-10 T, Avalon, USA /ECH2O-5, Decagon, USA	0, 0.02, 0.04, 0.1, 0.2, 0.4, 0.6, 1, 1.6, 2, 2.4	AV-10 T, Avalon, USA /ECH2O-5, Decagon, USA	0, 0.02, 0.04, 0.1, 0.2, 0.4, 0.6, 1
Rainfall	52,203, RM Young, USA	25	TE525MM, Campbell, USA	5

flux (W m^{-2}). Ignoring minor changes in ε, surface temperature change ΔT_s can be derived by the first derivative of Eq. (1):

$$\Delta T_s = \frac{1}{4\varepsilon\sigma T_s^3}[\underset{\text{I}}{\Delta S} + \underset{\text{II}}{\Delta L\downarrow} - \underset{\text{III}}{\Delta H} - \underset{\text{IV}}{\Delta\lambda E} - \underset{\text{V}}{\Delta G} - \underset{\text{VI}}{\Delta I}] \quad (4)$$

where Δ denotes the difference in a variable between the two sites (forest minus desert, so that positive values indicate warmer temperatures or more heat flux at the forest site). From Eq. (4), we can attribute the surface temperature changes ΔT_s due to biophysical changes in an albedo and incoming shortwave radiation component (term I), incoming longwave radiative forcing component (term II), sensible heat flux (term III), latent heat flux (term IV); ground heat flux (term V) and residual flux component (term VI), respectively. A detailed derivation of Eq. (4) was given in Supporting Information A1.

2.4. Boundary layer growth model

We further extended the analysis toward the PBL to investigate the climate impacts of vegetation cover change. The observed surface sensible and latent heat fluxes were coupled to a one-dimensional, clear-sky PBL model (McNaughton and Spriggs, 1986; Lhomme et al., 1998). Representing the convective boundary layer as a well-mixed slab of air of thickness h with constant profiles of potential temperature (θ) and specific humidity (q), the equation for heat and water balance are:

$$\rho C_p h\frac{d\theta}{dt} = H + \rho C_p(\theta_e - \theta)\frac{dh}{dt} \quad (5)$$

$$\rho h\frac{dq}{dt} = E + \rho(q_e - q)\frac{dh}{dt} \quad (6)$$

where ρ is the air density (kg m^{-3}); C_p is the specific heat capacity (J kg^{-1} K^{-1}); E is the evaporation flux at the surface (kg m^{-2} s^{-1}); and θ_e (K) and q_e (kg kg^{-1}) are the potential temperature and the specific humidity in the overlying undisturbed atmosphere, respectively. The rate of growth of the PBL is parameterized as (McNaughton and Spriggs, 1986):

$$\frac{dh}{dt} = \frac{H}{\rho C_p \gamma_\theta h} \quad (7)$$

where h is the current height of the boundary layer (m); and γ_θ is the gradient of the potential temperature just above the inversion base (K m^{-1}). The vertical profiles of potential temperature (θ_e) and specific humidity (q_e) in the overlying undisturbed atmosphere are assumed to be linear (Lhomme et al., 1998):

$$\theta_e = \gamma_\theta z + \theta_{e,0} = 4.78 \times 10^{-3} z + 293.6 \quad (8)$$

$$q_e = \gamma_q z + q_{e,0} = -2.85 \times 10^{-6} z + 0.01166 \quad (9)$$

where γ_q is the gradient of the specific humidity just above the PBL (kg kg^{-1} m^{-1}); z is the height above the ground (m); and $\theta_{e,0}$ and $q_{e,0}$ are the potential temperature and the specific humidity above the PBL extrapolated at $z = 0$. Eqs. (5), (6), and (7) have three dependent variables [$\theta(t)$, $q(t)$, $h(t)$] forming a set of three coupled first order differential equations, which are solved using the Runge-Kutta numerical method. The PBL model is initialized at sunrise (defined as first time step with positive net radiation) imposing fixed values of ρ, C_p, γ_θ, γ_q, $\theta_{e,0}$ and $q_{e,0}$, as well as initial PBL height $h_0 = 10$ m.

3. Results

3.1. Radiation balance and energy fluxes

The arid riparian forest showed large effects on the surface radiation balance (Fig. 2). The incoming shortwave radiation ($K\downarrow$) above the forest was similar to that above the background desert during the whole year period (Fig. 2a), but the albedo (α) of the forest was lower than that of the desert (i.e., $\Delta\alpha$ ranging from −0.05 to −0.15 with a mean of −0.08; Fig. 2b). The change of albedo due to forestation resulted in an increase in net surface shortwave radiation (S) above the forest (i.e., ΔS ranging from 7.27 to 18.3 W m^{-2} with a mean of 13.8 W m^{-2}; Fig. 2a). Longwave radiation is important for the arid ecosystems. We found that the incoming longwave radiation ($L\downarrow$) over the forest were higher than that over the desert ($\Delta L\downarrow$ ranging from 10.9 to 17.0 W m^{-2} with a mean of 13.9 W m^{-2}; Fig. 2a), indicating that there are some discrepancies in the atmospheric background over the two sites. The upwelling longwave radiation ($L\uparrow$) was nearly identical over the two sites from October to March, but a notable suppression of the upwelling longwave radiation was observed in the forest site from April to September (i.e., $\Delta L\uparrow$ ranging from −22.8 to −12.1 W m^{-2}) (Fig. 2a). Triggered by a combination of lower albedo, higher incoming longwave radiation and lower upwelling radiation, the net radiation (R_n) over the forest were considerably higher than that over the desert (i.e., ΔR_n ranging from 21.8 to 49.7 W m^{-2} with a mean of 35.4 W m^{-2}; Fig. 2a).

The partitioning of R_n into its different components (i.e., H, λE and G) differed significantly over the two sites (Fig. 2c). Due to the high plant transpiration potential from June to September, R_n was mostly consumed as λE at the forest sited during this period (i.e., with a mean ratio of λE to R_n being 0.93). On the contrary, H was the dominant turbulent flux throughout the year in the desert site (i.e., with a mean ratio of H to R_n being 0.79). Overall, the majority of R_n was consumed as H and λE at the two sites, and the contributions of G was small (<10 %; Fig. 2c).

3.2. Surface temperature and the biophysical effects

Fig. 3 showed the monthly variations of measured surface temperature (T_s) estimated from $L\uparrow$ at the two sites. The comparison suggested that the forest had a slightly warming effect (~ 0.5 °C) from November to February (hereafter named as warming-effect period), but exhibited a cooling role (i.e., ΔT_s ranging from −3.62 to −0.61 °C) from March to October (cooling-effect period). Overall, the annual mean T_s of the forest canopy is about 1.28 °C lower than that of the background desert.

We further used the DTM method to disentangle the contributions of different biophysical factors to surface climate. The calculated daily mean ΔT_s by the DTM method showed an excellent agreement with the observations (i.e., inserted plots in Fig. 4a and b for the cooling-effect and warming-effect periods, respectively), indicating that the DTM method is suitable for the ΔT_s partitioning calculations. It revealed that the latent heat flux component (term IV) played a dominant role in reducing the forest surface temperature (−14.5 ± 9.2 °C contribution to ΔT_s) during the cooling-effect period, while the sensible heat flux component (term III) together with the net surface shortwave radiation component (term I) and the incoming longwave radiation component (term II) tended to warm the surface temperature at the forest site (5.35 ± 7.37 °C, 2.55 ± 0.87 °C and 2.38 ± 1.90 °C for terms III, II and I, respectively; Fig. 4a). During the warming-effect period, the net surface shortwave radiation component (term I) and the incoming longwave radiation component (term II) were the main causes of rising the forest surface temperature (3.84 ± 1.55 °C and 3.04 ± 0.68 °C for terms I and II, respectively), while the latent heat flux component (term IV) and the sensible heat flux component (term III) acted to decrease the forest surface temperature (−1.03 ± 0.65 °C and − 0.68 ± 1.59 °C for terms IV and III, respectively; Fig. 4b). As expected, the ground heat flux component (term VI) generally remained smaller than other components in influencing ΔT_s during both periods (−0.71 ± 0.74 °C and 0.52 ± 0.49 °C for the cooling-effect and warming-effect periods, respectively). Noticeably, the contribution of the residual flux component (term VI) to ΔT_s was relatively large during the warming-effect period. This was mainly caused by the fact that the radiation and energy fluxes were relatively low during this period and thus the measurement errors may have significant effects on the final estimates.

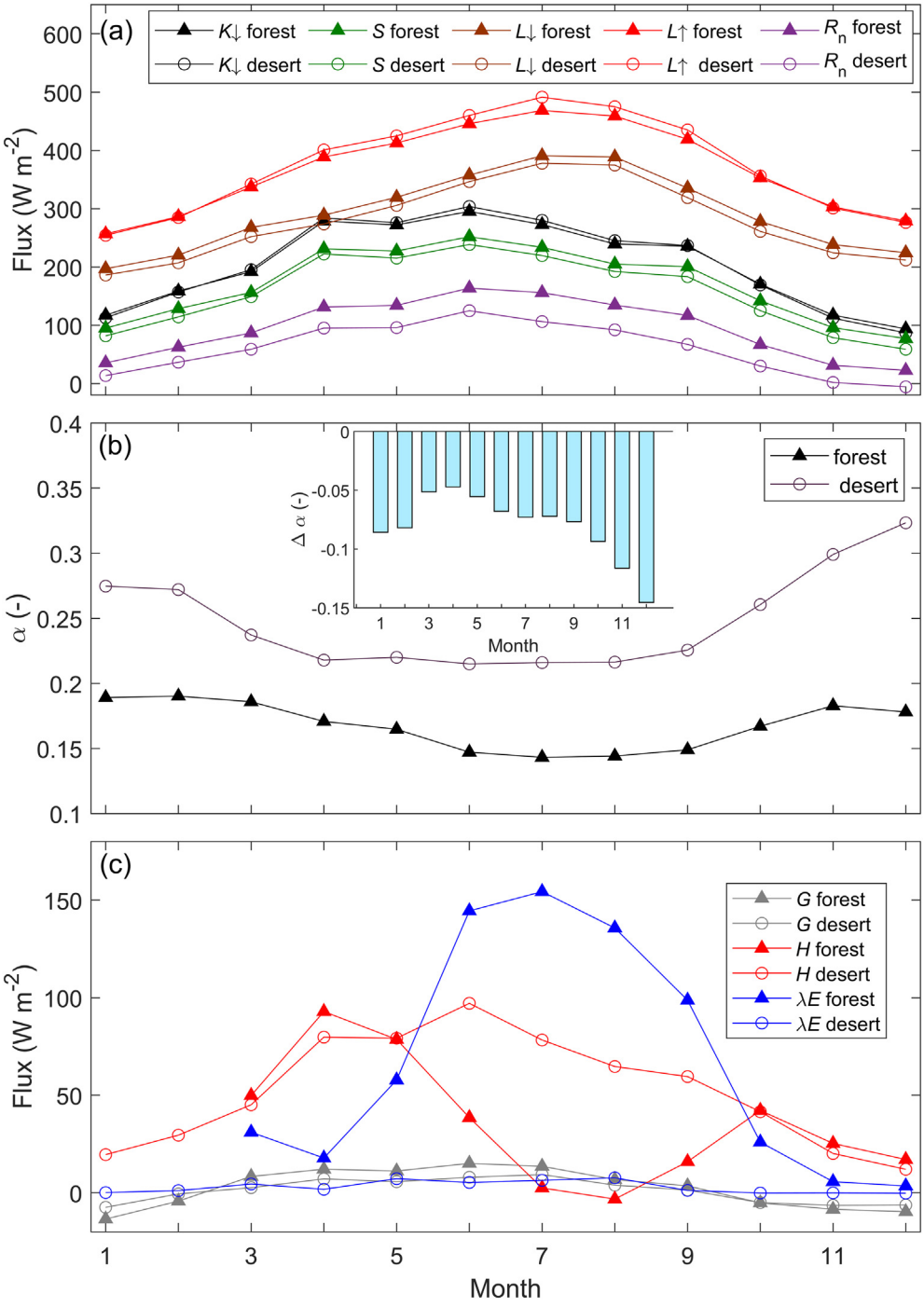

Fig. 2. Annual patterns in (a) radiation fluxes, (b) albedo, and (c) energy flux at the forest and desert site. These monthly means were calculated based in 0.5-hour values from eddy covariance and hydro-meteorological measurements.

3.3. Effects of vegetation cover change on PBL

To capture the effects of vegetation cover change on the climate system, we applied our measurements to the 1-D PBL model. Fig. 5 showed the diurnal variation of the idealized boundary layer variables (i.e., h, θ and q) over the two sites on a typical summer (1st August) and winter (1st November) day. On 1st August the sensible heat fluxes were low over the forest, thereby creating a PBL about 840 m shallower compared to that over the desert (Fig. 5a). Also, it was clear that the PBL over the forest was cooler (-1.38 K; Fig. 5b) and wetter (2.4 g kg^{-1}; Fig. 5c) than that over the desert. On 1st November the PBL over the forest was slightly deeper (212 m; Fig. 5e) and warmer (0.6 K; Fig. 5f) than that over the desert, but the dynamics of specific humidity were similar due to low latent heat fluxes over the two sites (Fig. 5g and h).

Fig. 6 showed the monthly variation of the boundary layer variables at the two sites. Due to the low sensible heat fluxes over the forest from June to September, the PBL over the forest was lower (Δh ranging from -621 m to -291 m; Fig. 6a), cooler ($\Delta\theta$ ranging from -0.33 K to -0.97 K; Fig. 6b) and wetter (Δq ranging from 1.10 g kg^{-1} to 1.98 g kg^{-1}; Fig. 6c) than that over the desert during this period. In contrast, the PBL over the forest was

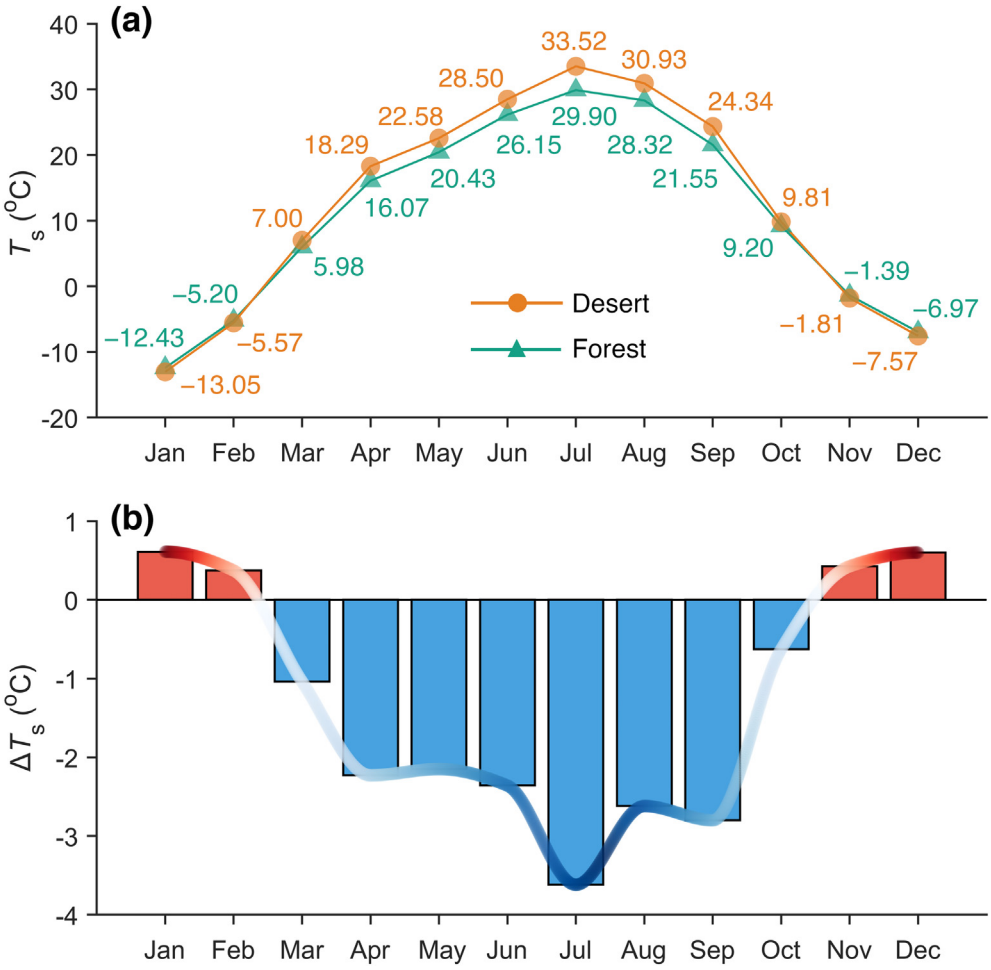

Fig. 3. (a) Annual patterns in surface temperature (T_s; °C) at the two sited. The numbers in brown represent the desert, and in green being forest; (b) the temperature difference between the two sites (ΔT_s; °C) with positive (negative) values indicating warmer (cooler) temperatures at the forest site compared to the background desert.

slightly deeper (Δh ranging from 134 m to 246 m; Fig. 6a) and warmer ($\Delta\theta$ ranging from 0.29 K to 0.58 K; Fig. 6b) than that over the desert, but the specific humidity was similar over the two site (Fig. 6c).

4. Discussion

4.1. Biophysical differences between sites

In analyzing the biophysical effects of afforest on climate, some researchers have assumed that the atmospheric background (i.e., the incoming shortwave/longwave radiations and air temperature) are similar at the paired sites (i.e., Lee et al., 2011; Peng et al., 2014). Hence, surface albedo (α) determines the amount of absorbed surface shortwave radiation, and is cited as the most influential factor in warming temperature (Betts, 2001; Davin and De Noblet-Ducoudre, 2010). However, we observed that the incoming longwave radiation ($L\downarrow$) over the forest site was considerably higher than that over the nearby desert (Fig. 2a), and ΔT_s caused by increased $L\downarrow$ were comparable to that due to changes in α (Fig. 4a and b). A similar phenomenon has been reported in previous studies (Broucke et al., 2015; Wang et al., 2018). What is the reason that $L\downarrow$ is higher over the forest site? The possible explanation is that water vapor in the PBL over the forest is higher than that over the desert background, as water vapor is the most important greenhouse gas and can limit the escape of longwave radiation through the atmosphere (Christy et al., 2006). Despite the absence of direct atmospheric humidity profile measurements, the 1-D PBL model showed that the PBL over the forest was generally wetter than that over the desert ($+0.65\ g\ kg^{-1}$ on annual basis; Fig. 6c). Thus, the PBL feedback alters the surface energy balance and further influences the surface temperature.

In addition to the effects of α and $L\downarrow$ on ΔT_s, energy partitioning has significant impacts on surface temperature and the development of the PBL (Davin and De Noblet-Ducoudre, 2010; Alexander, 2011). The partitioning of energy into its different components (i.e., H and λE) is mainly determined by land surface properties and water availability (Hemes et al., 2018). At the forest site, the groundwater table is shallow, and can be accessed by the roots of riparian plants (Su et al., 2022a, 2022b). On the other hand, soil moisture is strongly constrained at the desert due to sparse precipitation. Thus, the seasonal patterns in energy partitioning were different over the two sites (Fig. 2c). During the cooling-effect period, high λE over the forest (corresponding to a negative term IV) acted to cool surface, while low H (corresponding to a positive term III) caused a reduction in convective uplift and resulted in a warm temperature compared to the desert (Fig. 4a). During the warm-effect period, both λE and H over the forest were slightly higher (corresponding to negative terms IV and V) than that over the desert (Fig. 2c), and they (evaporative and convective surface cooling) acted together to reduce the forest surface temperature (Fig. 3b). Ideally, the residual flux component (term VI) should approach to zero, but this is almost never the case for observational data due to the energy imbalance problem with eddy covariance fluxes (Hemes et al., 2018). We used the Bowen ratio method to correct the measured sensible and latent heat fluxes (Foken, 2008), and recalculated the contributions of different biophysical factors to surface

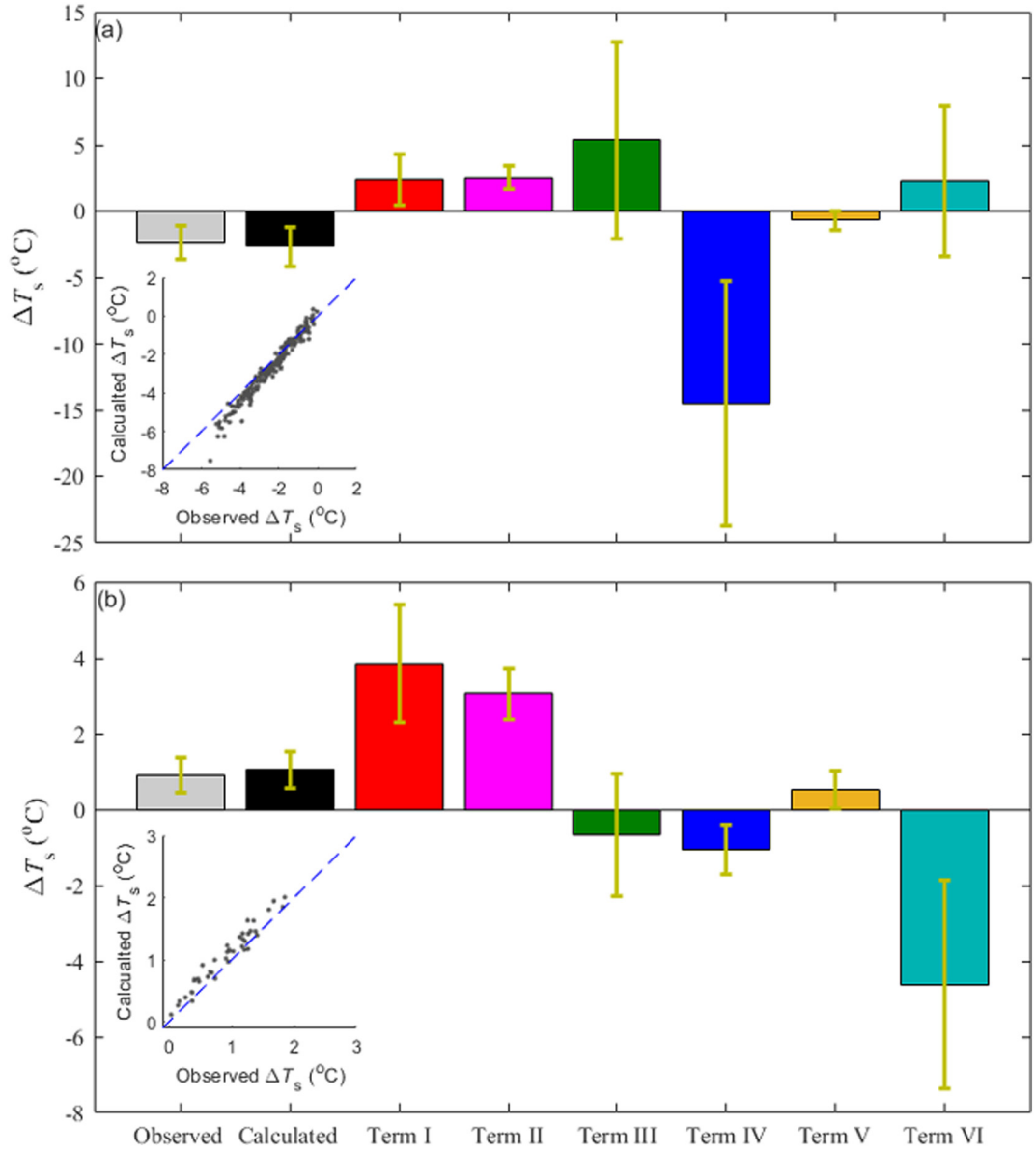

Fig. 4. Partition of the biophysical effect for the (a) cooling-effect period, and (b) warming-effect period using the DTM method. Error bars are given as 1 SE. The inset plots in (a) and (b) showed the relationships between observed and calculated ΔT_s.

climate. Similar results were obtained using the heat fluxes corrected for surface energy imbalance (see details in Supporting Information A2). Thus, the main conclusions of this study were not driven by the residual flux component (term VI).

4.2. Implications for vegetation and boundary layer

To capture the effects of afforestation on the climate system, we used a 1D-PBL model to calculate the state variables of the PBL (McNaughton and Spriggs, 1986; Lhomme et al., 1998). The simulated results indicated the PBL over the forest was shallower ($\Delta h = -448$ m), wetter ($\Delta q = 1.58$ g kg^{-1}) and cooler ($\Delta\theta = -0.68$ K) than that over the desert from June to September (the main plant growing seasons). However, the effects of afforestation in cooling the PBL were smaller compared to changes in surface temperature. A similar conclusion was drawn by Luyssaert et al. (2014) for temperature change from land management and land-cover change. During other months, the PBL over the forest was slightly higher ($\Delta h =$ 192 m) and warmer ($\Delta\theta = 0.46$ K) than that over the desert. This may be due to the fact that the forest has higher surface roughness (taller canopies) than desert. Enhanced surface roughness promotes greater mixing and heat dissipation (Lee et al., 2011). We calculated the aerodynamic conductance (G_{aero}; m s^{-1}), and found that G_{aero} over the forest were about 50 % higher than that over the desert (see details in Supporting Information A3).

In addition, the development of the PBL can give some critical feedbacks to surface energy balance and plant physiology (Baldocchi and Vogel, 1996). Therefore, the complex coupled feedbacks between surface layer and the PBL should be taken into account in assessments of climatic impact of land use change in future studies (Myhre et al., 2013; Hemes et al., 2018).

4.3. Policy implications and future work

Based on in situ observations, our study revealed that despite absorbing more radiation the arid riparian forest had a cooling effect on annual basis ($\Delta T_s = -1.28$ °C), but with a significant seasonality (i.e., slightly warming from November to February and cooling from March to October; Fig. 3). These results are consistent with previous studies based on in situ or satellite observations (Lee et al., 2011; Wickhama et al., 2012; Baldocchi and

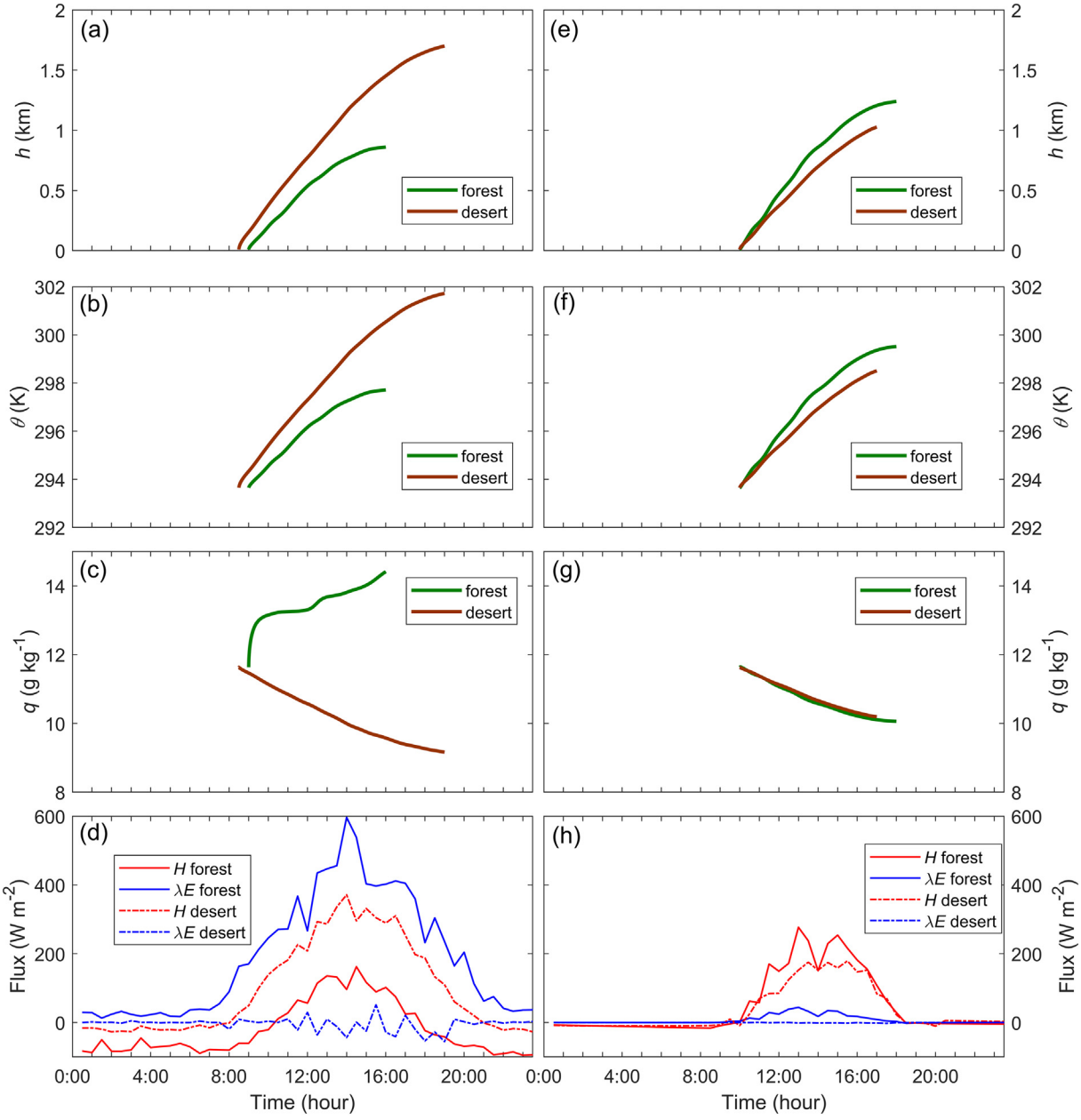

Fig. 5. Diurnal development of (a) the atmosphere boundary layer height (h; m), (b) potential temperature (θ; K), (c) specific humidity (q; g kg-1), and (d) observed surface sensible/latent heat fluxes over two sites on 1 August 2016. (e)-(h) were the same as (a)-(d), but on 1 November 2016.

Ma, 2013; Hemes et al., 2018). For examples, Lee et al. (2011) compared field-based measurements of surface air temperature for neighboring pairs of forested and open sites, and found that sites south of 45° N existed a weak seasonality with forests warmer than the open sites in January and slightly cooler in June. Baldocchi and Ma (2013) also reported that the air temperature difference over a site pair consisting of an oak savanna and an annual grassland in California exhibited a strong seasonal pattern. Therefore, the seasonality of ΔT_s should be taken into consideration in assessing how biophysical factors affect climate.

Overall, our results indicated that despite absorbing more net radiation the riparian forests have the potential to cool surface temperature (−1.28 °C) on annual basis, as compared to the desert background. Thus, the survivals of the riparian forests are very import for local people. However, it is well known that the riparian forest in arid and semi-arid regions mainly depend on groundwater for survivals (Rohde et al., 2021; Su et al., 2022a, 2022b). With the increases in human water demand, groundwater table has declined widely in arid regions (Haddeland et al., 2014). Thus, the long-term fate of the riparian forests in arid and semi-arid regions is mainly dependent on proper usages of the limited water resource (Rohde et al., 2021; Su et al., 2022a, 2022b). In the future, more studies on the ecology-water-economy relationship are needed to ensure a sustainable development in arid and semi-arid regions.

5. Conclusions

In this study, we investigated the biophysical effects of afforestation on climate in arid northwest China by using in situ observations and 1-D PBL model. Despite absorbing more net radiation (35.4 W m^{-2}), the riparian forests generally tended to cool the local surface temperature (−1.28 °C on annual basis) compared to the desert background. Interestingly, contrasting effects were observed at our site in different seasons. Specifically, afforestation may lead to a net cooling effect from March to September

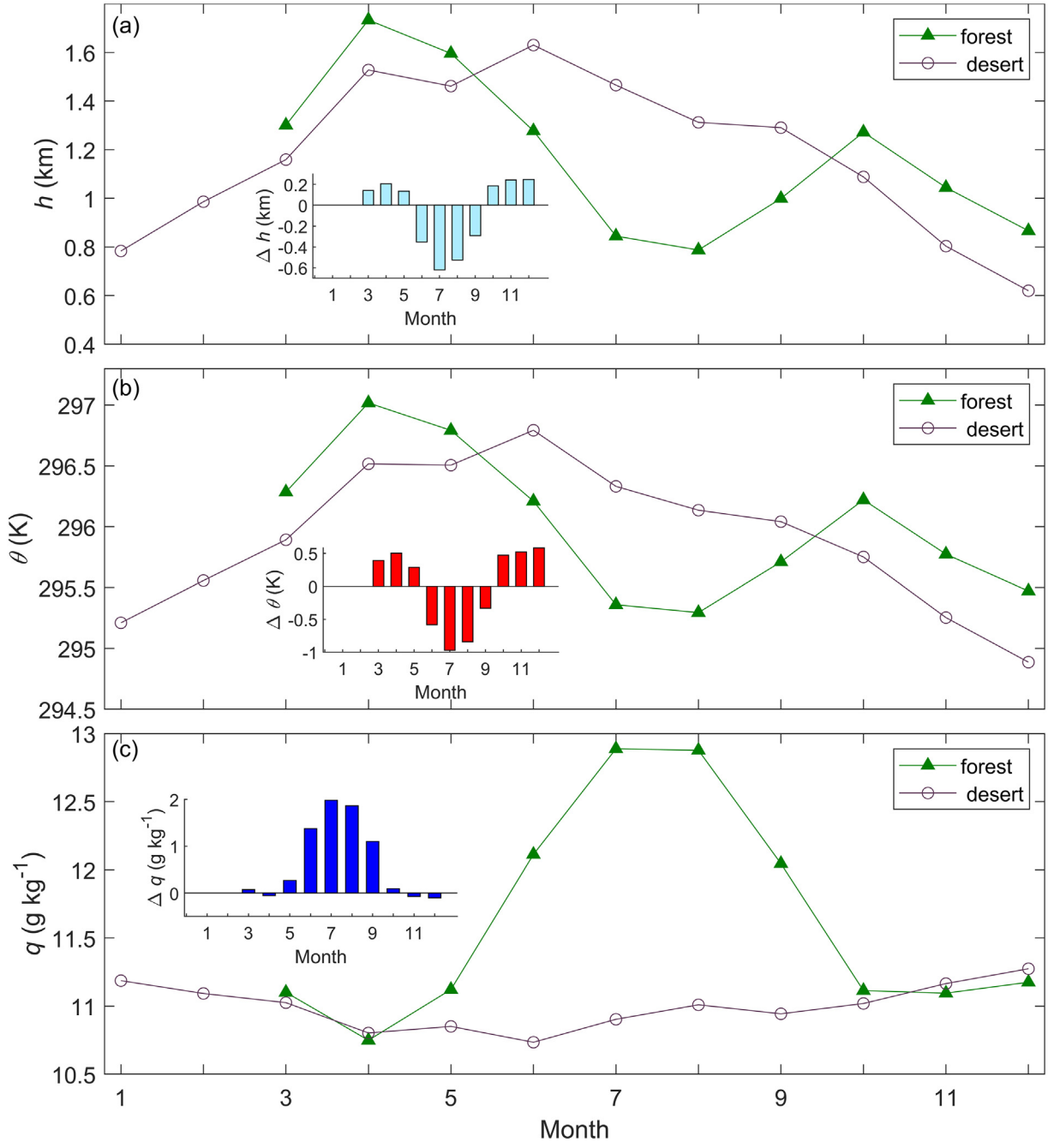

Fig. 6. Annual patterns in (a) the atmosphere boundary layer height (h; m), (b) potential temperature (θ; K), (c) specific humidity (q; g kg-1) at two sites. Noticeably, the sensible/latent heat fluxes were not available in January and February at the forest site. The inset plots in (a)-(c) showed the differences in h, θ and q between the two sites, respectively.

and a slightly warming effect in other months. The DTM method revealed that evapotranspiration played a dominant role in cooling surface temperature (-14.5 ± 9.2 °C) during the cooling-effect period, while α and $L\downarrow$ acted together to increase forest surface temperature (3.84 ± 1.55 °C and 3.04 ± 0.68 °C for α and $L\downarrow$, respectively) during the warming-effect period.

Reduced diurnal H inputs to the PBL over forest from June to September resulted in shallower, cooler and wetter boundary layers compared to background desert. An increase in atmospheric moisture would potentially increase cloud cover and result in a substantially higher $L\downarrow$. Therefore, the complex coupled feedbacks between surface layer and the PBL can alter the land surface energy balance and surface temperature. From October to May, the diurnal H inputs to the PBL over the forest were similar to that over desert. Due to high aerodynamic conductance, the PBL was slightly deeper and warmer over the forest than that over the desert, but with similar specific humidity. In the future, more attentions should be paid to protect the riparian forests and ensure a sustainable development in arid regions.

CRediT authorship contribution statement

The paper was mainly organized and written by Dr. Su Yonghong; Luo Fandi was responsible for data analysis; The code used in this paper was written by Prof. Zhu Gaofeng; The field observations were made by Zhang Qi.

Data availability

The data used in this study are available from the National Tibetan Plateau/Third Pole Environment Data Center (http://data.tpdc.ac.cn).

Declaration of competing interest

We declared that we have no financial and personal relationships with other people or organizations that can inappropriately influence our work. All authors have agreed the submits of this paper to your Journal. We declared that we will not submit this paper to another Journal until we hear from you.

Acknowledgements

The authors would thank Dr. Daniel S Alessi (Associate Editor) for his continued help during the revisions of the paper. We also thank the anonymous reviews for their critical reviews and helpful comments. This research was founded by the National Natural Science Foundation of China (Nos. 42071138, 41871078 and 42171019).

Appendix A. Supplementary data

Supplementary data to this article can be found online at https://doi.org/10.1016/j.scitotenv.2022.160856.

References

Alexander, L., 2011. Extreme heat rooted in dry soils. Nat. Geosci. 4, 12–13.
Alkama, R., Cescatti, A., 2016. Biophysical climate impacts of recent changes in global forest cover. Science 351, 600–603.
Anderson, R.G., Canadell, J.G., Randerson, J.T., Jackson, R.B., Hungate, B.A., Baldocchi, D.D., Ban-Weiss, G.A., Bonan, G.B., Caldeira, K., Cao, L., Diffenbaugh, N.S., Gurney, K.R., Kueppers, L.M., Law, B.E., Luyssaert, S., O'Halloran, T.L., 2011. Biophysical considerations in forestry forclimate protection. Front. Ecol. Environ. 9 (3), 174–182.
Bala, G., Caldeira, K., Wickett, M., Phillips, T.J., Lobell, D.B., Delire, C., Mirin, A., 2007. Combined climate and carbon-cycle effects of large-scale deforestation. Proc. Natl. Acad. Sci. U. S. A. 104 (16), 6550–6555.
Baldocchi, D.D., Ma, S., 2013. How will land use affect air temperature in the surface boundary layer? Lessons learned from a comparative study on the energy balance of an oak savanna and annual grassland in California, USA. Tellus B 65 (1). https://doi.org/10.3402/tellusb.v65i0.19994.
Baldocchi, D.D., Vogel, C., 1996. A comparative study of water vapor, energy and CO2 flux densities above and below a temperate broadleaf and a boreal pine forest. Tree Physiol. 16, 5–16.
Betts, R.A., 2000. Offset of the potential carbon sink from boreal forestation by decreases in surface albedo. Nature 408, 187–190.
Betts, R.A., 2001. Biogeophysical impacts of land use on present-day climate: near-surface temperature change and radiative forcing. Atmos. Sci. Lett. https://doi.org/10.1006/asle.2001.0023.
Bonan, G.B., 2008. Forests and climate change: forcings, feedbacks, and the climate benefits of forests. Science 320, 1444–1449.
Bonan, G.B., Pollard, D., Thompson, S.L., 1992. Effects of boreal forest vegetation on global climate. Nature 359, 716–718.
Broucke, V.S., Luyssaert, S., Davin, E.L., Janssens, I., van Lipzig, N., 2015. New insights in the capability of climate models to simulate the impact of LUC based on temperature decomposition of paired site observations. J. Geophys. Res. Atmos. 120, 5417–5436.
Burakowski, E., Tawfik, A., Ouimette, A., Lepine, L., Novick, Ki, Ollinger, S., Zarzycki, C., Bonan, G., 2018. The role of surface roughness, albedo, and Bowen ratio on ecosystem energy balance in the eastern United States. Agric. For. Meteorol. 249, 367–376.
Christy, J.R., Norris, W.B., Redmond, K., Gallo, K.P., 2006. Methodology and results of calculating central California surface temperature trends: evidence of human-induced climate change? J. Clim. 19 (4), 548–563.
Davin, E.L., De Noblet-Ducoudre, N., 2010. Climatic impact of global-scale deforestation: radiative versus non-radiative processes. J. Clim. 23, 97–112.
De Frenne, P., et al., 2013. Microclimate moderates plant responses to macroclimate warming. PNAS 110 (46), 18561–18565.
Findell, K.L., Knutson, T.R., Milly, P.C.D., 2006. Weak simulated extratropical responses to complete tropical deforestation. J. Clim. 19, 2835–2850.
Foken, T., 2008. The energy balance closure problem: an overview. Ecol. Appl. 18 (6), 1351–1367.
Haddeland, I., Heinke, J., Biemans, H., Eisner, S., Flörke, M., Hanasaki, N., Konzmann, M., Ludwig, F., Masaki, Y., Schewe, J., Stacke, T., Tessler, Z.D., Wada, Y., Wisser, D., 2014. Global water resources affected by human interventions and climate change. Proc. Natl. Acad. Sci. 111 (9), 3251–3256.
Heimann, M., Reichstein, M., 2008. Terrestrial ecosystem carbon dynamics and climate feedbacks. Nature 451, 289–292.
Hemes, K.S., Eichelmann, E., Chamberlain, S.D., Knox, S.H., Oikawa, P.Y., Sturtevant, C., Verfaillie, J., Szutu, D., Baldocchi, D.D., 2018. A unique combination of aerodynamic and surface properties contribute to surface cooling in restored wetlands of the Sacramento-San Joaquin Delta, California. J. Geophys. Res. Biogeosci. 123, 2072–2090.
Juang, J.-Y., Katul, G., Siqueira, M., Stoy, P., Novick, K., 2007. Separating the effects of albedo from eco-physiological changes on surface temperature along a successional chronosequence in the southeastern United States. Geophys. Res. Lett. 34, L21408.
Lal, R., 2004. Carbon sequestration in dryland ecosystems. Environ. Manag. 33 (4), 528–544.
Lawrence, D., Vandecar, K., 2015. Effects of tropical deforestation on climate and agriculture. Nat. Clim. Chang. 5, 27–36.
Lawrence, D., Coe, M., Walker, W., Verchot, L., Vandecar, L., 2022. The unseen effects of deforestation: biophysical effects on climate. Front. For. Glob. Chang. 5, 756115. https://doi.org/10.3389/ffgc.2022.756115.
Lean, J., Warrilow, D., 1989. Simulation of the regional climatic impact of Amazon deforestation. Nature 342, 411–413.
Lee, X.H., et al., 2011. Observed increase in local cooling effect of deforestation at higher latitudes. Nature 479, 384–387.
Lhomme, J.P., Elguero, E., Chehbouni, A., Boulet, G., 1998. Stomatal control of transpiration: examination of Monteith's formulation of canopy resistance. Water Resour. Res. 34, 2301–2308.
Li, X., Cheng, G.D., Liu, S.M., Xiao, Q., Ma, M.G., Jin, R., Che, T., Liu, Q.H., Wang, W.Z., Qi, Y., Wen, J.G., Li, H.Y., Zhu, G.F., Guo, J.W., Ran, Y.H., Wang, S.G., Zhu, Z.L., Zhou, J., Hu, X.L., Xu, Z.W., 2013. Heihe watershed allied telemetry experimental research (HiWATER): scientific objectives and experimental design. Bull. Am. Meteorol. Soc. 94, 1145–1160.
Li, Y., Zhao, M., Motesharrei, S., Mu, Q., Kalnay, E., Li, S., 2015. Local cooling and warming effects of forests based on satellite observations. Nat. Commun. 6, 6603. https://doi.org/10.1038/ncomms7603.
Li, Y., Brando, P.M., Morton, D.C., Lawrence, D.M., Yang, H., Randerson, J.T., 2022. Deforestation-induced climate change reduces carbon storage in remaining tropical forests. Nat. Commun. 13 (1), 1964. https://doi.org/10.1038/s41467-022-29601-0.
Liu, S.M., Xu, Z.W., Song, L.S., Zhao, Q.Y., Ge, Y., Xu, T.R., Ma, Y.F., Zhu, Z.L., Jia, Z.Z., Zhang, F., 2016. Upscaling evapotranspiration measurements from multi-site to the satellite pixel scale over heterogeneous land surfaces. Agric. For. Meteorol. 230–231, 97–113.
Luyssaert, S., et al., 2014. Land management and land-cover change have impacts of similar magnitude on surface temperature. Nat. Clim. Chang. 4 (5), 389–393.
McNaughton, K.G., Spriggs, T.W., 1986. A mixed-layer model for regional evaporation. Boundary-Layer Meteorol. 34, 243–262.
Myhre, G., Shindell, D., Bréon, F.-M., Collins, W., Fuglestvedt, J., Huang, J., et al., 2013. 2013: Anthropogenic and natural radiative forcing. In: Stocker, T.F., et al. (Eds.), Climate change 2013: The Physical Science Basis. Contribution of Working Group I to the Fifth Assessment Report of the Intergovernmental Panel on Climate Change. Cambridge University Press, Cambridge, UK and New York, pp. 659–740 Chap. 8.
Peng, S.S., Piao, S.L., Zeng, Z.Z., Ciais, P., Zhou, L.M., Li, L.Z.X., Myneni, R.B., Yin, Y., Zeng, H., 2014. Afforestation in China cools local land surface temperature. PNAS 111 (8), 2915–2919.
Rohde, M.M., Stella, J.C., Roberts, D.A., Singer, M.B., 2021. Groundwater dependence of riparian woodlands and the disrupting effect of anthropogenically altered streamflow. Proc. Natl. Acad. Sci. 118 (25), e2026453118. https://doi.org/10.1073/pnas.2026453118.
Rotenberg, E., Yakir, D., 2010. Contributions of semi-arid forests to the climate system. Science 327, 451–454.
Si, J., Feng, Q., Wen, X., Xi, H., Yu, T., Li, W., Zhao, C., 2015. Modeling soil water content in extreme arid area using an adaptive neuro-fuzzy inference system. J. Hydrol. 527, 679–687.
Su, Y., Feng, Q., Zhu, G., Wang, Y., Zhang, Q., 2022b. A new method of estimating groundwater evapotranspiration at sub-daily scale using water table fluctuations. Water 14, 876. https://doi.org/10.3390/w14060876.
Su, Y.H., Feng, Q., Zhu, G.F., 2007. Identification and evolution of groundwater chemistry in the Ejin Sub-basin of the Heihe River, Northwest China. Pedosphere 17, 331–342.
Su, Y.H., Feng, Q., Zhu, G.F., Zhang, Q., 2022a. Evaluating the different methods for estimating groundwater evapotranspiration using diurnal water table fluctuations. J. Hydrol. 607, 127508. https://doi.org/10.1016/j.jhydrol.2022.127508.
Wang, F., Liang, R.J., Yang, X.L., Chen, M.J., 2002. A study of ecological water requirements in northwest China I: theoretical analysis. J. Nat. Resour. 17, 1–8 [In Chinese].
Wang, L., Lee, X., Schultz, N., Chen, S., Wei, Z., Fu, C., Lin, G., 2018. Response of surface temperature to afforestation in the Kubuqi Desert, Inner Mongolia. J. Geophys. Res. Atmos. 123, 948–964.
Wang, Y., Zhou, J., Ma, R., Zhu, G., Zhang, Y., 2022. Development of a new pedotransfer function addressing limitations in soil hydraulic models and observations. Water Resour. Res. 58, e2021WR031406. https://doi.org/10.1029/2021WR031406.
Wickhama, J.D., Wadea, T.G., Riitters, K.H., 2012. Comparison of cropland and forest surface temperatures across the conterminous United States. Agric. For. Meteorol. 166–167, 137–143.
Xu, Z., Liu, S., Zhu, Z., Zhou, J., Shi, W., Xu, T., Yang, F., Zhang, Y., He, X., 2020. Exploring evapotranspiration changes in a typical endorheic basin through the integrated observatory network. Agric. For. Meteorol. 290, 108010. https://doi.org/10.1016/j.agrformet.2020.108010.
Xu, Z.W., Ma, Y.F., Liu, S.M., Shi, W.J., Wang, J.M., 2017. Assessment of the energy balance closure under advective conditions and its impact using remote sensing data. J. Appl. Meteorol. Clim. 56, 127–140.
Zhang, M., Lee, X.H., Yu, G.R., Han, S.J., Wang, H.M., Yan, J.H., Zhang, Y.P., Li, Y.D., Ohta, T., Hirano, T., Kim, J., Yoshifuji, N., Wang, W., 2014. Response of surface air temperature to small-scale land clearing across latitudes. Environ. Res. Lett. 9, 1–7.